In-Plane Cyclic Testing of Concrete-Filled Sandwich Steel Panel Walls with and without Boundary Elements

Yasser Alzeni, M.ASCE[1]; and Michel Bruneau, F.ASCE[2]

Abstract: Concrete-filled sandwich steel panel (CFSSP) walls are composed of two steel skin plates interconnected by tie bars, with the space between the skin plates filled with concrete. These walls are attractive for use in seismic regions, but limited knowledge exists on their in-plane cycling inelastic flexural behavior. This paper reports results from an experimental study investigating this behavior by testing four cantilever CFSSP walls with and without circular boundary elements, having length-to-width ratios of 2.46 and 2.76, respectively. All of the tested walls were able to exceed their theoretical plastic moment capacity, calculated assuming a full plastic stress distribution of the cross section. The tested specimens exhibited stable ductile behavior up to 3% drift (and beyond in some conditions). Local buckling of the steel skin led to minor degradation in flexural strength. Fracture of the skin plates eventually developed as the ultimate failure mode. The effect of using different tie bars spacing to steel plate thickness ratios, and different techniques for welding the tie bars to the skin plates, are also addressed. **DOI: 10.1061/(ASCE)ST.1943-541X.0001791.**

Author keywords: Cyclic testing; Composite behavior; Sandwich wall; Steel; Concrete; Seismic; Boundary element; Flexural plastic strength; Metal and composite structures.

Introduction

Concrete-filled sandwich steel panel (CFSSP) walls are being considered by practicing engineers for construction in seismic regions of the United States, including as ductile flexural walls in high-rise applications. Their appeal is that they are envisioned to be highly ductile, redundant, of high strength, and easy and rapid to construct (overcoming the congestion of reinforcement details that can be encountered in ordinary reinforced concrete walls, and because the steel shell can be used as formwork). Beyond accelerated construction and ductile seismic performance, use of a CFSSP wall instead of a conventional reinforced concrete wall in building applications can translate into thinner walls with resulting greater leasable space. However, there is a critical lack of knowledge on the in-plane cyclic inelastic behavior of such CFSSP walls, which, in spite of all the positive attributes of the structural system, is an absolute impediment to their implementation in seismic regions.

To help understand the in-plane flexural behavior of such walls, in the current study four specimens with and without boundary elements were subjected to cyclic inelastic loading. Performance was evaluated in terms of ductility and lateral load-carrying capacity. The results of this experimental work are presented here.

However, before proceeding further, a clarification in terminology is in order. At the time this research was conducted, the terminology *walls with boundary elements* was used to refer to the presence of a distinct structural shape wider than the rest of the wall [namely, a full hollow structural section (HSS) here] by opposition to the case where a simple closure plate (square or half-circular) is used at the end of the wall (referred to here as walls without boundary elements). This terminology is kept here to ensure consistency with the information contained in the full research report (Alzeni and Bruneau 2014) because changing the names of specimens and terminology here would only serve to confuse the readers referring to this report. The connectivity with this broader report should not be destroyed. However, it is anticipated that in the AISC 341-16 (AISC 2016) seismic provisions, the term *boundary elements* will be used in a manner that encompasses both types of walls tested here, and the term *walls without boundary elements* will refer to those that do not have such cap plates (built, for example, using formwork at their ends to contain the concrete within the wall during the pour). This is consistent with the terminology defined in Kurt et al. (2016) in which walls without boundary elements do not include flanges, end walls, or other types of boundary elements. The reader should therefore be aware that the AISC-specific terminology would consider all walls tested here as having boundary elements (albeit different types of boundary elements).

Literature Review

Various types of composite shear walls have been considered in the past. In a first type, structural steel sections have been used as boundary elements to replace the vertical reinforcing bars in conventional concrete walls, but still using confining ties in the boundary regions of the wall. Cho et al. (2004), Dan et al. (2011), and Liao et al. (2012) (among many) investigated the behavior of such concrete walls reinforced by vertical steel sections. In a second type, the steel plate infill of steel plate shear walls (SPSWs) was tied to reinforced concrete panels on one or both sides of the steel web plate with shear studs. Zhao and Astaneh-Asl (2004) investigated the cyclic behavior of such SPSW made composite by adding precast reinforced concrete panels bolted to the steel web infill; in this structural system, ductile performance of the SPSW was achieved through shear yielding of the steel panel, although Lin

[1]Assistant Professor, Dept. of Structural Engineering, Alexandria Univ., Alexandria, Egypt (corresponding author). E-mail: yasser_alzeni@azizmi.com

[2]Professor, Dept. of Civil and Environmental Engineering, Univ. at Buffalo, The State Univ. of New York, 212 Ketter Hall, Buffalo, NY 14260. E-mail: bruneau@buffalo.edu

Note. This manuscript was submitted on April 29, 2015; approved on January 4, 2017; published online on June 21, 2017. Discussion period open until November 21, 2017; separate discussions must be submitted for individual papers. This paper is part of the ***Journal of Structural Engineering***, © ASCE, ISSN 0733-9445.

and Tsai (2004) showed that this strength may not be achieved in some instances. Rahai and Hatami (2009) conducted an analytical study on the aforementioned walls to evaluate the effect of variation of shear studs spacing.

The type of composite wall considered here consists of sandwich steel panels filled with concrete. These have been used in many applications and research on that structural system has largely focused on walls subjected to out-of-plane loading and/or noncyclic behavior. For example, Wright (1998) investigated the behavior of a composite wall system composed of two skins of profiled steel and concrete infill subjected to axial loads and out-of-plane bending moment; Hossain and Wright (1998) tested five composite panels under in-plane shear and developed equations for estimation of the strength and stiffness of walls; and for steel-composite (SC) composite walls used as an alternative to conventional RC walls in safety-related nuclear facilities, Varma et al. (2014) developed both a mechanical-based model, and a detailed nonlinear finite-element model for predicting the behavior and failure of the SC wall panels subjected to a combination of in-plane forces. Sener and Varma (2014) summarized the experimental database of the SC shear tests under different load combinations, considered different design parameters, compared the out-of-plane shear strength from the experimental database with the shear strength calculated based on the current applicable codes, and presented a suggestion for the shear strength reduction factor (φ). Sener et al. (2016) summarized the experimental database of out-of-plane flexural tests conducted on SC walls under different loading configurations and different design parameters, compared the experimental flexural strength with that estimated by the applicable design codes, and suggested a strength reduction factor (φ) for the out-of-plane flexure.

Some of the past research has been conducted in relation to the Bi-Steel (TATA steel, London, U.K.) sandwich system that has been developed as flooring system, beams, columns, and wall system used in some nonseismic regions (Corus 2003, 2007).

Limited research has been conducted on the in-plane inelastic cyclic response of CFSSP walls. Eom et al. (2009) conducted in-plane cyclic testing of three individual walls and two coupled walls having rectangular and T-shaped cross sections, representing 1/3- and 1/4-scale models of the first stories of a 30-story prototype. The aspect ratio of the isolated wall was 3.7, intended to ensure a dominant in-plane flexural behavior. The tested specimen showed premature failure in the corner welding of the rectangular section and different methods were used to strengthen the walls, which were retested and (in some cases) able achieve estimated peak loads and develop reasonable ductile performance. Epackachi et al. (2014) tested four CFSSP walls having an aspect ratio of 1, but having no cap plate at the cross-section ends. Under in-plane cyclic loading, the tested walls were able to reach their yield moment (equal to M_y) and failed in a flexural mode, while the hysteretic loops exhibited significant pinching. Kurt et al. (2016) tested eight CFSSP walls without boundary elements under cyclic lateral loads, where the walls had an aspect ratio between 0.6 and 1.0; the lateral load capacity of the tested walls were governed by the in-plane flexure capacity of wall cross section at the base. Kurt et al. (2016) discussed the differences in behavior between walls with and without boundary elements. The walls without boundary elements were defined as walls that do not have any boundary elements, flanges, or end walls, and their lateral resistance capacity is defined by their ability to resist an interaction of shear forces and overturning moments. While in the case of composite walls with boundary elements, the in-plane shear is resisted by the web of the wall while the overturning moment is resisted by the flange and boundary elements. Seo et al. (2016) used a mechanics-based model (MBM) to present the fundamental in-plane shear force–shear strain (V–γ) of the SC walls, compared the results with the results of the experimental database, and introduced an estimated value for the strength reduction factor (φ).

Review of the existing literature indicates that there are only limited data available on the inelastic cyclic behavior of flexural CFSSP walls. The research presented in this paper focuses on walls having aspect ratios larger than 2, intended to attain their plastic moment capacity and exhibit reasonable ductile performance, considering different spacing of tie bars to steel plate thickness ratios, different methods of welding the tie bars to the skin plate, details to avoid premature failures at the wall's corners due large strains, and investigating the effect of using boundary elements [concrete filled tubes (CFTs)] for the CFSSP walls.

Experimental Program

Four large-scale CFSSP wall specimens were designed as cantilever walls fixed to a reinforced concrete footing; early staging of construction of a walls and its concrete foundation is shown in Fig. 1. The CFSSP walls tested as part of this research program were meant to be representative of implementation in commercial buildings as cantilevering walls surrounded by gravity frames, where the floor is tied to the walls through seismic collectors. The findings from this research cannot be directly extrapolated to designs for walls having T or C shaped plane cross section, or other more complex configurations, for which additional research is recommended.

The specimens' dimensions were selected to be representative of walls that have a dominant flexure behavior in the context of multistory buildings. The aspect ratio and dimension were selected to ensure that the tested cross section would develop its flexural limit state (full plastic moment) without yielding in shear. Walls of greater aspect ratios would be similarly flexure-dominant. Although the walls were not designed to be representative of a specific prototype, the selected aspect ratio was no less than for similar walls typically built in multistory buildings in nonseismic regions (Bowerman et al. 1999).

The tested specimens were divided over two groups. In the first group, identified by the label NB, the CFSSP walls have no boundary elements and their cross section is composed of double web skin plates having thickness, t, of 8 mm and web width, b, of 1,016 mm, connected through circular tie bars spaced equally in both horizontal and vertical directions at a spacing, S, equal to 203.2 and 304.8 mm for Specimens CFSSP-NB1 and CFSSP-NB2, respectively, corresponding to S/t ratio of 25.6 and 38.4. The cross section is closed at its ends by half-HSS sections; these were used instead of square ends in order to avoid premature failure of the cross section's corner welds due to concentration of stresses that has been observed in prior research on composite rectangular sections (e.g., Eom et al. 2009; El-Bahey and Bruneau 2011; Ge and Usami 1996; Usami and Ge 1994; Kawashima and Unjoh 1997). Both specimens of Group NB have the same outer dimensions, plate thicknesses, and total width and height. Specimen CFSSP-NB1 and CFSSP-NB2 have a total width, W, of 1,235.1 mm (skin plates plus two half-HSS 8.625×0.325) and total thickness, t_t, of 219.1 mm. The height of both specimens in Group NB is 3,048 mm above the top of their footing, resulting in an aspect ratio (height to total cross-section depth), h/W, of 2.47. For specimens in Group NB, the tie bars were welded to the web skin plate using plug welding: tie bars having a total length equal to [total thickness of the wall (t_t) − thickness of the steel plates (t_s)] were positioned to span the distance between the steel

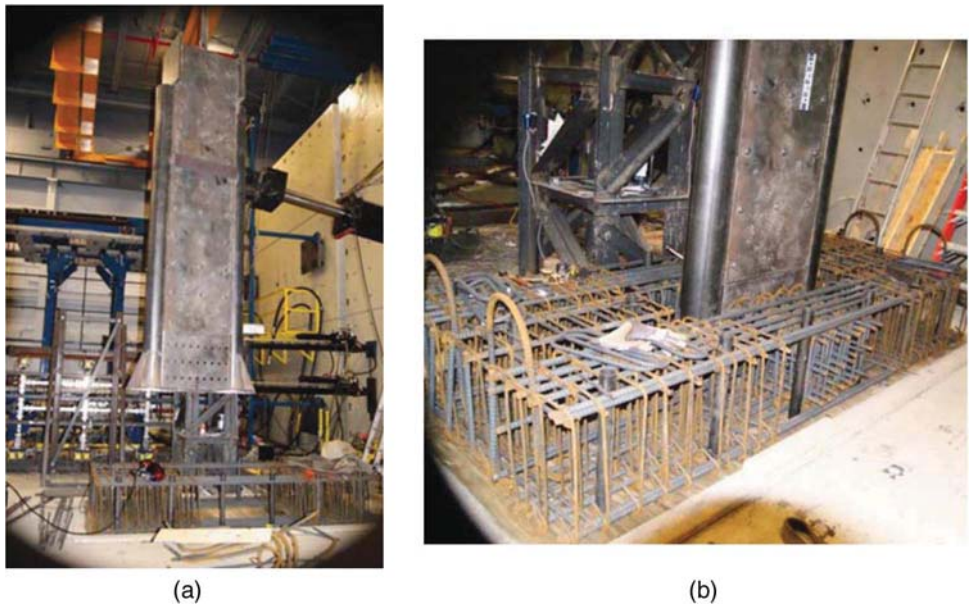

Fig. 1. Construction of the tested specimens: (a) placement of specimen in foundation; (b) connection between wall and foundation

web plates center lines, and the remaining half-thickness of the plate on each side was filled with welding material to create the plug weld. The tie bars had a diameter of 25.4 mm and were designed to remain elastic throughout the test.

The second group of tested specimens, identified by the label B, are CFSSP walls having boundary elements (i.e., complete structural shapes) consisting of a concrete-filled round HSS section. The walls' cross section consists of HSS columns and of double web skin plates having a width, L, of 762 mm, a thickness, t_s, of 8 mm, and connected through tie bars spaced equally in both horizontal and vertical directions at a spacing, S, of 203.2 and 304.8 mm for Specimens CFSSP-B1 and CFSSP-B2, respectively, corresponding to S/t ratios of 25.6 and 38.4 (i.e., the same values used for the NB specimens). The two specimens in Group B have a h/W of 2.76. The Specimen CFSSP-B1 tie bars were connected to the web plate using plug welding as described for the Group NB specimens. However, for Specimen CFSSP-B2, tie bars were assembled differently. Bars having a total length of $(t_t + 2t_s)$ were used. As such, when installed, the tie bars protruded a distance of 8 mm beyond the steel web plate on each side, and were fillet welded to the web steel plates.

Fig. 2 shows the cross sections of all specimens. A summary of the tested specimens' properties is presented in Table 1. The proposed system is intended to develop its full plastic moment capacity, M_P. Therefore, the CFSSP wall skin plates and HSS must be prevented from local buckling prior to full development of M_P (understandably, beyond the yield point, local buckling will unavoidably develop during cycling inelastic response, but if sufficiently delayed, adequate ductile response can be developed). Accordingly, the HSS part of the cross section was chosen to comply with the AISC 341-10 (AISC 2010) limit specified for moderately ductile members, namely

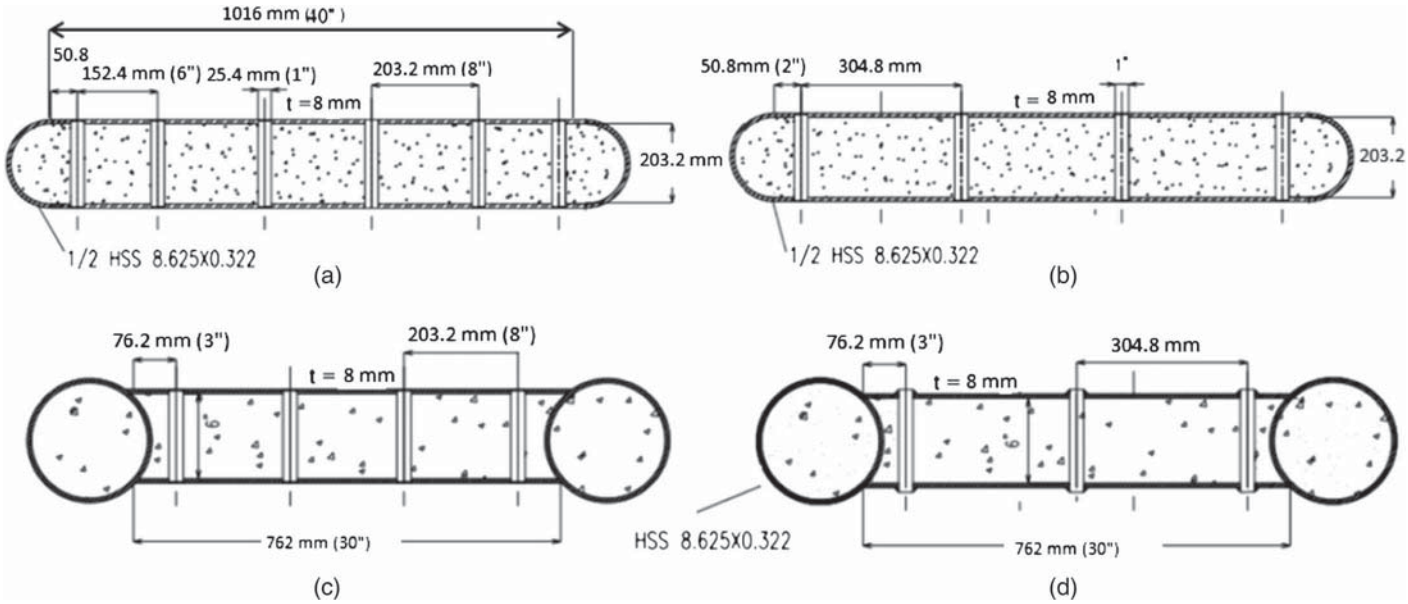

Fig. 2. Tested specimens of CFSSP walls: (a) CFSSP-NB1; (b) CFSSP-NB2; (c) CFSSP-B1; (d) CFSSP-B2

Table 1. Parameters for Tested Specimens

Specimens	Web plate, F_y b (mm)	t_s (mm)	Boundary	D (mm)	t (mm)	t_c (mm)	S (mm)	S/t	W (mm)	h/W	Welding of tie bars
CFSSP-NB1	1,016	8	Half-HSS 8.625 × 0.322	219.1	8.18	203.2	203.2	25.6	123.5	2.47	Plug
CFSSP-NB2	1,016	8		219.1	8.18	203.2	304.8	25.6	123.5	2.47	Plug
CFSSP-B1	762	8	HSS 8.625 × 0.322	219.1	8.18	152.4	203.2	38.4	110.4	2.76	Plug
CFSSP-B2	762	8		219.1	8.18	152.4	304.8	38.4	110.4	2.76	Fillet

$$D/t_{\mathrm{HSS}} < 0.44E/F_y \quad (1)$$

All steel panels were built by a certified steel fabricator in the Buffalo, New York, area. For the Group NB specimens, the half-HSS 8.622 × 0.322 used at their end was cut from a full HSS using water jet cutting to avoid overheating of the HSS, which could lead to distortions or changing of material properties of the HSS.

The skin plates were then assembled. Temporary internal spacers and bolts were used while the tie bars were welded in position. The half-HSS (for Group NB specimens) or full HSS (for Group B specimens) were then welded to the web plates using full penetration groove welding. No backup bars were necessary for this weld. This represents only one possible way to fabricate these walls. The commentary to AISC 341-16 provides some fabrication alternatives for connecting the ties. Overall, the multiple advantages of flexural-dominant CFSSP walls in terms of cost-savings, accelerated construction time, ease of transportation to the construction site (which is straightforward because wall panels are typically stacked on a flatbed truck), and convenience in using the walls as formwork are progressively being recognized; as a consequence, the structural system is being implemented in some major projects already. Fig. 3 shows fabrication of the tested specimens.

The approach taken to determine the vertical and horizontal spacing of the tie bars, w_1 and w_2, respectively, such as to similarly prevent the skin plates from experiencing local buckling before yielding, was to consider the plate as similar to the case in which a compression flange in the concrete-filled section is subjected to uniform compression and has simply supported edges for which Wright (1995) showed that the S/t ratio should be less than or equal

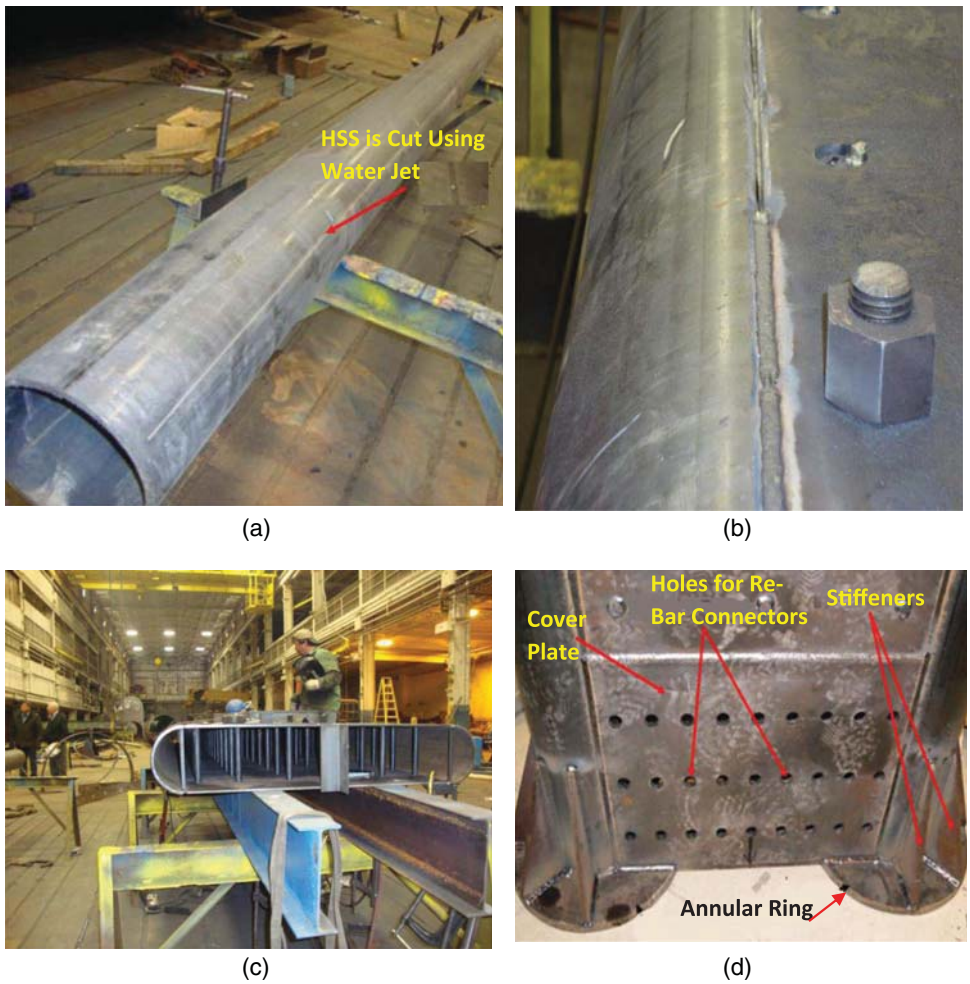

Fig. 3. Fabrication of the tested specimen: (a) water jet cutting of HSS; (b) welding between half-HSS and steel web plate; (c) assembly of CFSSP-NB1 specimen; (d) base of Specimen CFSSP-B1

Table 2. Material Properties for Tested Specimens

Specimens	HSS, F_y (MPa)	Web, F_y (MPa)	HSS, F_u (MPa)	Web, $F_uFF_uF_y$ (MPa)	Concrete, f'_c (MPa)
CFSSP-NB1	289.6	434.4	420.6	499.9	47.9
CFSSP-NB2	296.5	420.6	427.5	510.2	46.8
CFSSP-B1	303.4	427.5	448.2	493	48.8
CFSSP-B2	317.2	441.3	420.6	530.9	32.9

to 37 to ensure ductile behavior. Also, as an alternative and simpler approach, considering the plate as an idealized fixed-ends column and setting the critical stress equal to the nominal yield stress of the web plate, a S/t value of 43 was obtained. Zhang et al. (2014) presented the effect of shear connectors design on the level of composite action in the steel-composite (SC) walls and the maximum steel plate slenderness needed to prevent local buckling of the steel plates prior to yielding.

For the CFSSP walls tested in this research, for a maximum 304.8-mm (12-in.) spacing of tie bars and web plates thickness of 7.94 mm (5/16 in.), the corresponding maximum S/t ratio used for the specimens was 38.4. This is approximately equal to the previous value for plates having simply supported edges.

The diameter of the tie bars should be selected such that they can provide adequate stiffness to control local buckling of the web plates, resist the shearing force transferred between the reinforced concrete core and the steel skin plate, and have adequate strength to resist the tensile force that develops during formation of the plastic mechanism created during inelastic buckling of the web skin plate.

Stiffness of the ties was not quantified here because it was believed to not be a controlling parameter for these specimens (and possibly not controlling either for most applications, although the authors do not have supporting data to that effect; this could be the subject of future research). Also, given the large number of ties typically used in the walls, the ties shear strength was also not expected to govern design either.

Past experiments have showed the undesirable rapid wall strength and stiffness degradation (e.g., Ramesh et al. 2013) that occurs when ties fail. The ties diameter was determined in accordance with the requirements in Section H7 of AISC-341-16, which provide conservative axial demands in the ties to avoid possible premature tie failures.

The welding between the tie bars and the skin plates (either plug welds or fillet welds, depending on the specimen) was sized to resist the same calculated tensile force in the tie bars.

The concrete used for the four specimens was self-consolidating concrete (SCC), with a slump of 76.2 mm. This concrete was used because of its high workability. For Specimen CFSSP-B2, steel fibers of 50.8 mm (2 in.) were added to the SCC as an attempt to better distribute tension cracking of the concrete and possibly improve its ductility.

The steel used for the HSS was ASTM A252 (ASTM 2010) Grade 3 and for the steel web plates was ASTM A572 (ASTM 2015) Grade 50. Coupon test results gave an average yield strength of 427.5 MPa (62 ksi) for the steel used in the web plate, and 296.5 MPa (43 ksi) for the round HSS. The steel in the CFSSP walls specimens here amounted to 7.7% of the total cross-section area; while there is no reason to believe that the findings from this study would not be applicable for other reinforcement ratios, the results should not be excessively extrapolated.

Table 2 summarizes the material properties for Groups NB and B in terms of average values for the material properties obtained from concrete cylinder tests and steel coupon tests. Fig. 4 shows the results for the coupon test on the HSS and steel web plate of Specimen CFSSP-NB2. All the tested coupons have shown the same stress-strain curve pattern where the HSS steel did not show a clear yield point and was determined using the 0.2% offset method, while the steel web plates have shown a clear yield plateau. All concrete cylinders were a standard size of 150 mm in diameter and 300 mm in length, and steel coupons were prepared in accordance with ASTM A370 (ASTM 2017) with 200-mm gauge lengths. Three cylinders were tested for each specimen together with two coupon tests for steel used (i.e., plates and HSS) in each specimen. Concrete was ordered from local suppliers with no specific requirements other than specifying a self-consolidating concrete having a 27.6 MPa (4 ksi) compressive strength (leaving mix design to the supplier). Further details on the material properties are provided in Alzeni and Bruneau (2014).

Strains were measured using axial strain gauges and rosettes located at different points on the steel skin of the tested specimens along cross sections located at 304.8 mm (12 in.) and 508 mm (20 in.) above the top of the foundation. Displacement potentiometers were used to measure in-plane movements at different locations along the height of the specimens. LVDTs were located at the extreme fibers of the tested specimens (HSS part of the cross section) and used to calculate rotations at the base of the tested specimens, which are used in calculating wall curvature. A krypton dynamic measurement system was used to record and measure displacement fields for nodes on the web of the skin plates.

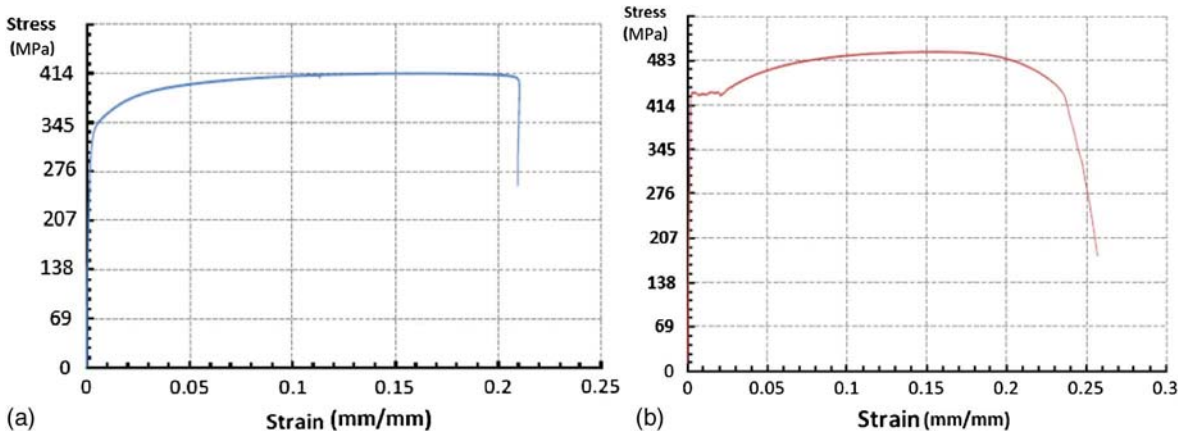

Fig. 4. Coupon test results, CFSSP-NB2, for (a) HSS boundary elements; (b) steel web plates

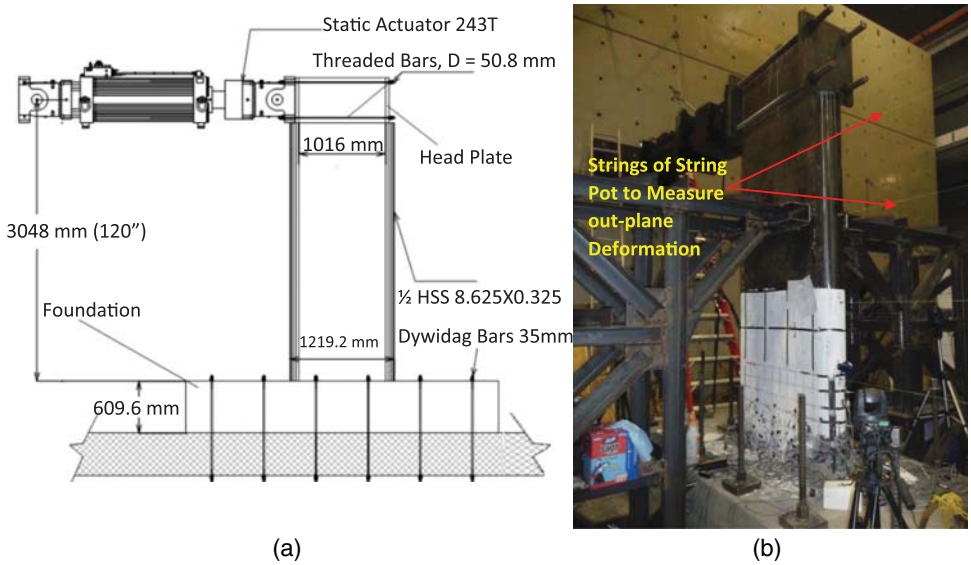

Fig. 5. Test setup: (a) elevation of tested specimen; (b) test rig

Boundary elements are expected to be used when larger cross sections are needed at the ends of the walls to resist large seismic demands. Both types of the tested walls are expected to sustain axial gravity loads that would not exceed 20% of their nominal axial capacity. However, it is recognized that the tested specimens were not subjected to axial load and that this could be the subject of future research. Also, the diaphragms in the structure are connected to the wall through seismic collectors. Methods to connect the surrounding framing to the walls have been developed and experimentally validated by Ramesh et al. (2013).

Test Setup and Loading Protocol

The tested specimens were cantilever-type walls fixed to a reinforced concrete base, itself connected to the strong floor of the laboratory using pretensioned DYWIDAG bars (DSI, New York), as shown in Fig. 5. Lateral loading was applied at the top of the specimens by a servocontrolled actuator. The size of the foundation and the pretension force in the DYWIDAG bars were selected so as to prevent uplift of the reinforced concrete foundation, and it was designed to remain elastic throughout the testing. To design all elements of the test setup (foundations, connection with foundation, and test setup components), the plastic moment value was multiplied by a factor of 1.5 to account for expected values of yield strength higher than nominal values and for the development of strain hardening in the steel elements in the CFSSP walls during testing. As shown in Fig. 6(a), at the wall web, reinforcing bars were passed through holes in the part of the wall that was embedded in the foundation. These bars were subjected to shearing forces generated at the interface between steel and concrete. Considering rebars transferring shearing forces to be #8 rebars, having a diameter of 25.4 mm (1 in.), the number of rebars was calculated based on the rebar shearing force needed to transfer the tensile stress distribution in the web at 1.5 M_p and to transfer the corresponding horizontal force at the base of the wall.

The forces generated due to yielding of the HSS part of the cross section required another form of connectors to transfer the tension forces at the toe of the CFSSP walls to the footing. For this purpose, an annular ring was used following the concept proposed by

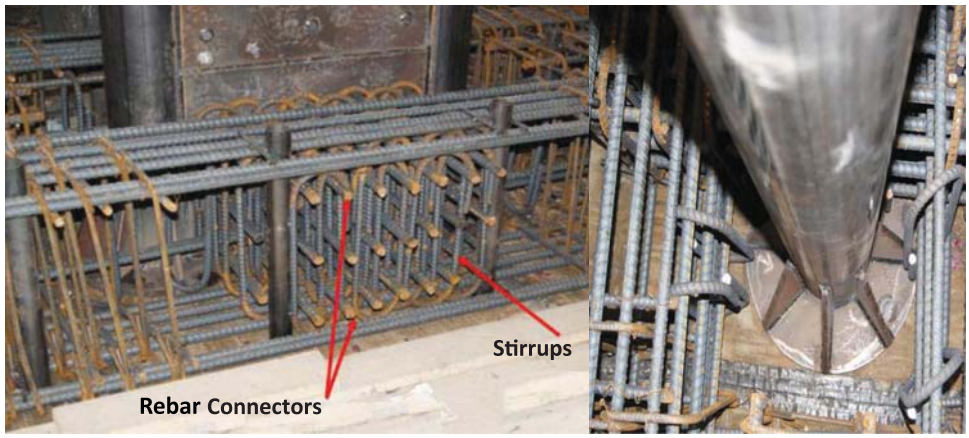

Fig. 6. Wall-to-footing connection: (a) web rebar connectors; (b) stiffened annular ring at HSS base

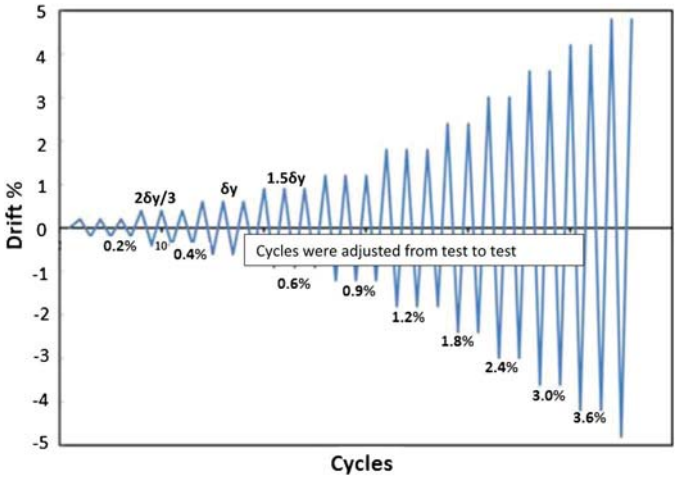

Fig. 7. Loading protocol

Roeder et al. (2003). More specifically, when the half-HSS forming the flange of the CFSSP-NB (and full HSS of CFSSP-B) yields in tension, the strategy adopted here consisted of transferring this tension yield force to the foundation through an annular ring welded at the base of the half-circular (or full HSS) section. Roeder et al. commented that some of that force might be transferred through shear friction along the face of the steel, but the design approach adopted here was to neglect this possible contribution and rely instead on vertical stirrups intersecting the concrete cone pullup surface. The thickness of the annular ring required was calculated to be 25.4 mm (1 in.); stiffeners were used to minimize the annular ring thickness. The annular ring used is shown in Fig. 6(b).

Details on the wall connection to the footing and actuator connection are provided in Alzeni and Bruneau (2014). Two bracing trusses were used to avoid out-of-plane motion of the wall.

Specimens were subjected to quasi-static displacement cycles following the ATC 24 (ATC 1992) loading protocol, with three displacement cycles at each displacement step, up to a displacement equal to three times the yield displacement, and two cycles at each displacement magnitude after that. The yield displacement, δ_y, was initially defined here as the displacement at which the extreme steel fibers of the CFSSP wall skin plate starts to yield. The values of δ_y were obtained from pushover analyses done using the finite-element models (in *ABAQUS*), considering a fixed-base model.

The loading protocol, shown in Fig. 7, was adapted during the test to experimentally define the yield displacement of the tested CFSSP walls based on observation of the recorded hysteretic curves. The specimens were subjected to cyclic displacements according to this protocol until substantial fracture in the steel web plates and the HSS part of the CFSSP wall specimens occurred.

Experimental Results

The experimentally obtained lateral load versus top displacement relationships are shown in Fig. 8. The corresponding yield displacement, δ_y, maximum displacement, maximum strength compared to M_p calculated based on coupon values, and dissipated energy are summarized in Table 3. The displacement ductility reported in that table was calculated based on a definition of δ_y established by considering an equivalent bilinear system. The maximum displacement was defined as the postpeak displacement where the strength degrades to 80% of the peak value.

Group NB Specimens

Following are some observations made during testing of Specimen CFSSP-NB1. At a drift of 1.2%, the moment acting on the wall cross section was 36,220 kN-m (32,058 kip-in.), which represents 100% of the plastic moment capacity of the wall cross section M_p (calculated as described subsequently). At 1.8% drift, during the first cycle of loading, a moment of 41,330 kN-m (36,480 kip-in.) was developed at the wall base, which is equivalent to 114% of M_p, and local buckling of the steel web plate of Specimen CFSSP-NB1 was observed. Buckling started between the first and the second row of tie bars from the base, as shown in Fig. 9(a). Flaking of the white wash paint occurred on the perimeter of some of the first- and second-row tie bars from the base. The apex of the local buckling wave was approximately located middistance between the first and second row of tie bars from the face of foundation.

At 2.4% drift, a base moment of 41,041 kN-m (36,324 kip-in.) was developed, corresponding to 113.6% M_P, and the half-HSS part of the CFSSP-NB1 specimen developed local buckling as an extension of the web plate local buckling, as shown in Fig. 9(b). Cracks developed in the plug welds of the first row of tie bars; those cracks developed along the circumference of the tie bars, with projected horizontal lengths that ranged from between the full diameter of the tie in the tie bars closer to the wall ends, to half-diameter cracks for the tie bars further from the ends, as shown in Fig. 9(c).

At 3% lateral drift, the wall still resisted 111% M_P. The amplitude of local buckling became more significant. Fracture developed on the full perimeter of other tie bars, and started to propagate horizontally into the web plate from the circumference of the first tie bar in the first row, and toward the half-HSS. At 3.6% drift, flexural strength dropped to 78.2% of M_P. A first crack developed in the HSS part of the cross section, initiating at the middle of the buckled wave in the half-HSS section at one end of the wall. After the second cycle at this displacement drift, at the other end of the wall, fractures also propagated from the tie bars on the first row of tie bars, through the centerline of the first row of tie bars, as shown in Fig. 9(d). There were no deformations or fractures observed in the tie bars themselves.

The test was stopped after the second cycle at a displacement equivalent to 3.6% drift; the residual flexural strength at that point was 40.5% of M_p. During this step, the wall fractured along a significant percentage of its base, in a plane passing through the center line of the first row of tie bars, over a distance of approximately 457.2 mm (18 in.) at one end of the wall. At the other end, the fracture in the HSS section remained located in the middle of the buckled wave, while a second fracture in the web extended through the centerline of the first row of tie bars. Removal of the wall revealed that the concrete in the vicinity of the locally buckled skin plate was crushed.

The behavior of Specimen CFSSP-NB2 was essentially similar, with the following notable differences: (1) half-diameter fracture of the plug weld of the first row of tie bars was noticed at 1.8% drift; (2) fractures in some of the plug welds along the first row of tie bars (typically located in the upper half of the tie bars) started to propagate in the web plates at 2.4% drift; (3) at 3% drift, flexural strength was 104% of M_P, corresponding to a 8.66% drop from the peak value obtained at 1.8% drift; (4) at 3.6% drift, flexural strength dropped to 71% of M_P, the crack that developed in the HSS propagated below the local buckling wave of the HSS, and, in the final cycles at this drift, some crushed concrete escaped through the cracks in the CFSSP-NB1 skin; (5) at 4.0% drift, the specimen resisted 38.7% of M_P; and (6) testing continued with displacement

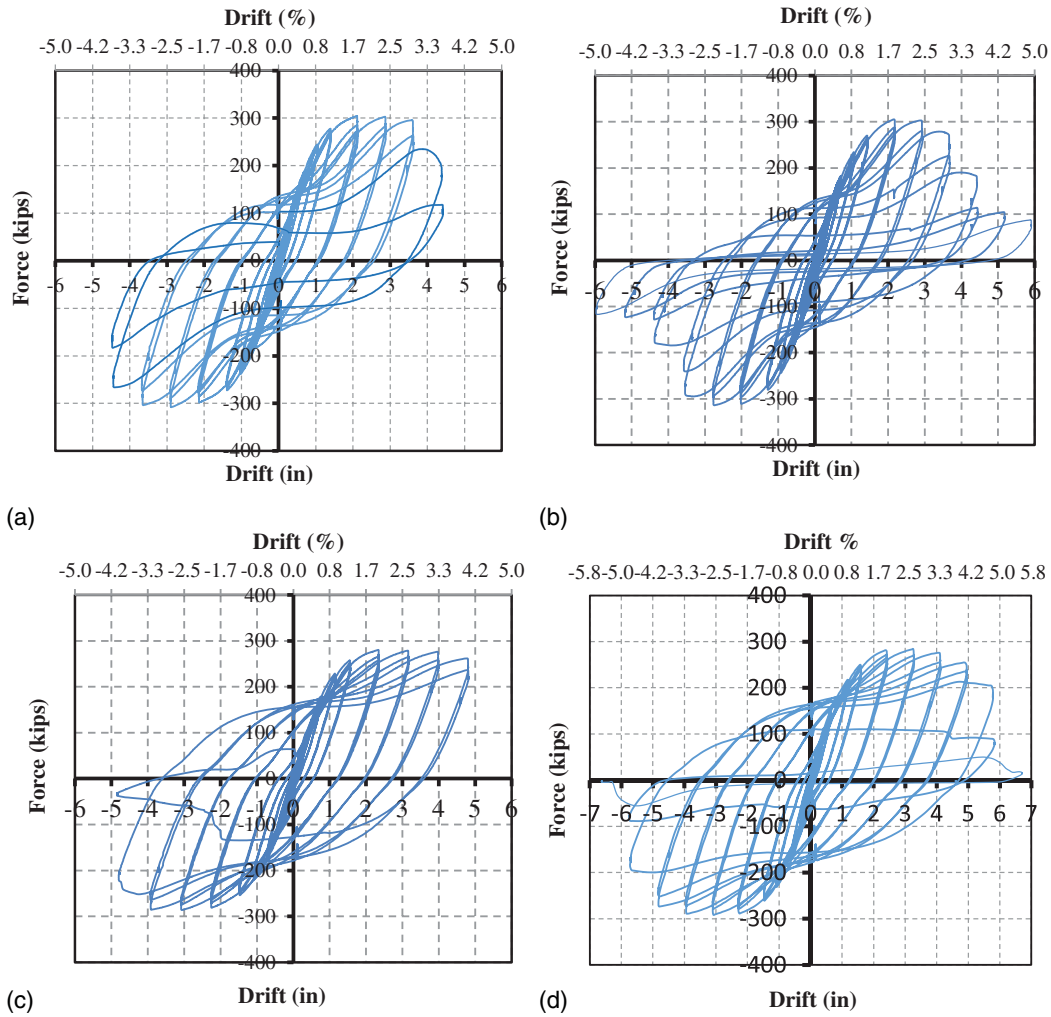

Fig. 8. Force displacement relationships for the tested specimens: (a) CFSSP-NB1; (b) CFSSP-NB2; (c) CFSSP-B1; (d) CFSSP-B2

Table 3. Evaluation of Test Data

Specimens	Maximum displacement[a] Δ_u (mm)	Maximum drift[a] Δ_u/h (%)	Yield displacement Δ_y (mm)	Ductility ratio Δ_u/Δ_y	μ (first yield) Φ_{max}/Φ_{y1}	μ (bilinear) Φ_{max}/Φ_{yb}	Dissipated energy (kN-m)
CFSSP-NB1	104.1	3.4	20.3	5.13	14.44	7.74	1,349
CFSSP-NB2	93.2	3.0	25.4	3.67	12.88	6.54	1,821
CFSSP-B1	121.9	4.0	22.9	5.33	14.98	8	1,595
CFSSP-B2	127	4.16	22.9	5.50	11.06	5.55	1,965

[a]At the point beyond M_{max} where strength has dropped to $0.8M_{max}$.

cycles in steps of 0.5% drift up to 7.2% drift (to record progressive strength degradation as the cracks propagated until they cumulatively reached one-third of the total cross-section depth, although those extreme cycles are not shown in Fig. 7, at which point Specimen CFSSP-NB2 was only able to resist 30% of its plastic moment and the test was stopped. Fig. 9(f) shows the fracture at the base of Specimen CFSSP-NB2 at 4.3% drift.

Group B Specimens

The cyclic displacement protocol used for specimens of Group B was slightly different from the one used for Group NB specimens due to a 12% difference in the estimated yield displacement, δ_y.

Behavior of Specimen CFSSP-B1 is first described. At a lateral drift of 1%, a moment of 30,912 kN-m (27,360 kip-in.) was resisted by the specimen, which corresponds to M_P. At 1.33% drift, the specimen reached a moment of 34,919 kN-m (30,907 kip-in.), which corresponds to 113% of M_P. There was no visual evidence of local buckling.

At 2% drift, at a flexural strength of 123% of M_P, the first observation was made of cracks initiating along the plug welds in the first row of tie bars. The web plate of the CFSSP-B1 specimen started to locally buckle, as shown in Fig. 9(g). with a buckling wave spanning the distance between the first and second horizontal rows of bars, and the apex of the buckled wave at middistance of

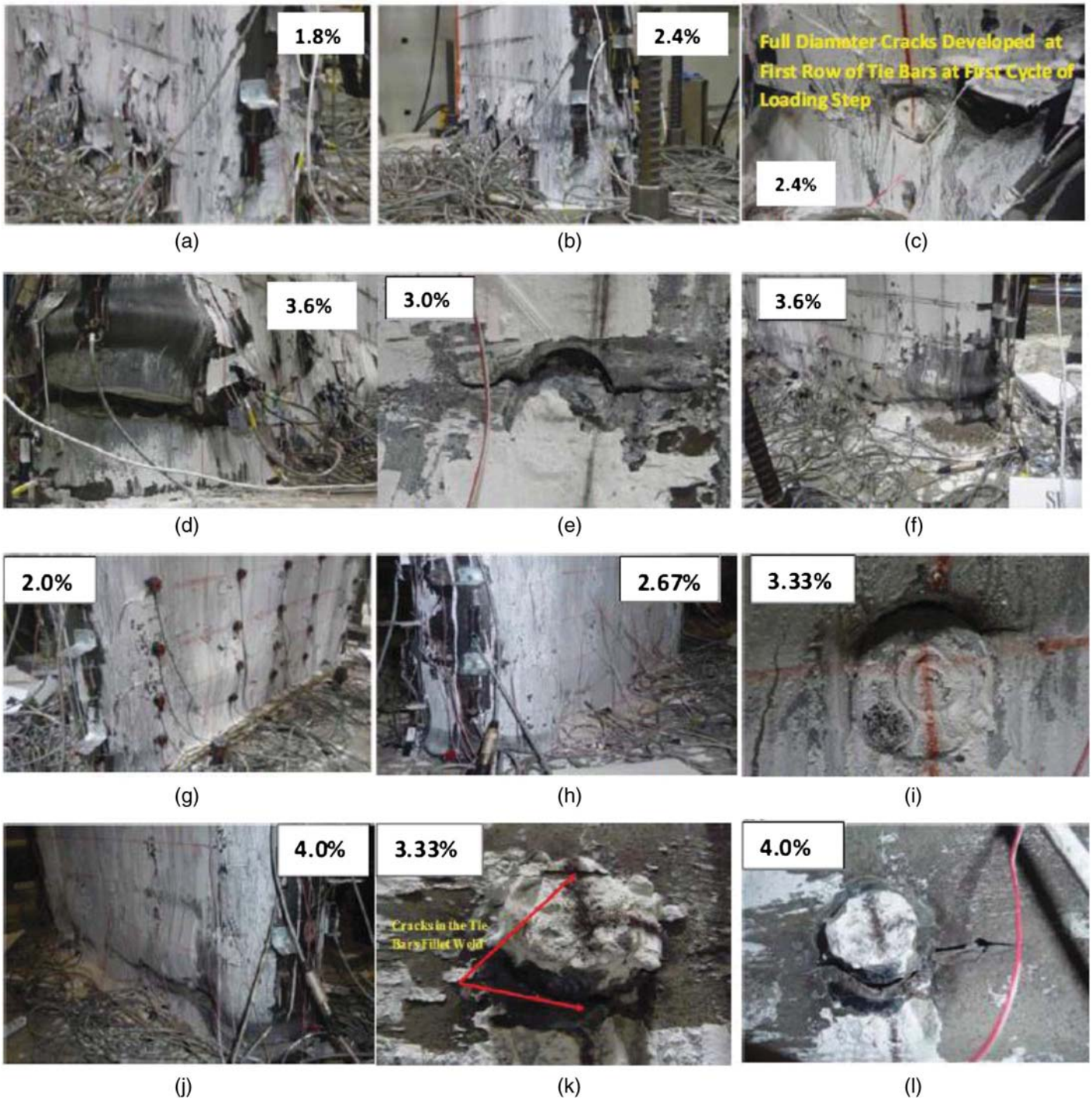

Fig. 9. Local buckling and failure modes of the tested specimens at different drift perecent values: (a) web local buckling of CFSSP-NB1; (b) local buckling of HSS CFSSP-NB1; (c) fracture in tie bars weld of CFSSP-NB1; (d) fracture of CFSSP-NB1; (e) fracture propagation of CFSSP-NB2; (f) fracture of CFSSP-NB2; (g) web local buckling of CFSSP-B1; (h) HSS local buckling of CFSSP-B1; (i) fracture of plug welding of CFSSP-B1; (j) fracture of CFSSP-B1; (k) cracks in weld of CFSSP-B2; (l) propagation of cracks of CFSSP-B2

these two rows. The HSS part of the cross section also exhibited the onset of local buckling (but the buckling waves were too small to be captured by photos).

At 2.67% drift, the specimen still resisted 122% of M_P, but the HSS boundary elements of the specimen showed local buckling at their base. Local buckling of the steel web plates and the HSS section were not linked (i.e., they occurred at different elevations), and the local buckling of the HSS part of the wall developed over the entire visible HSS perimeter, as shown in Fig. 9(h).

At 3.33% drift, the flexural strength was still 121% of M_P. Fracture of the tie bars plug welds further developed, up to a horizontal projection length of full- or half-diameter of the tie bars. Some of the cracks propagated from the circumference of the tie bars into the web plate. The longest cracks extended 44.45 mm (1 3/4 in.) into the steel web, as shown in Fig. 9(i). Some crushed concrete spilled from the open cracks in the specimen's skin.

The specimen's flexural strength was 115% of M_P during the first cycle of displacement at 4% drift. After that, the specimen's

strength started to degrade rapidly and testing stopped at 5% drift, where the strength of the wall was approximately 50% of the peak value and the wall was fractured at the level of the first row of tie bars for almost 508 mm (20 in.) as shown in Fig. 9(j). The specimen was cut along the fractured zone. The concrete in the vicinity of the buckled steel plates was found to be crushed, but still soundeed closer to the cross-section midthickness.

Specimen CFSSP-B2 behaved similarly, with the following significant differences. At 2% drift, no cracks were observed in the fillet welds of the tie bars; the onset of web local buckling also occurred at this stage, and the specimen exhibited a strength of 38,368 kN-m (33,960 kip-in.), which corresponds to 123% of M_P. At 2.67% drift, the specimen reached its peak flexural strength, corresponding to 125% of M_P. The steel web local buckling wave started at the first row of tie bars and extended up to two-thirds of the vertical spacing of tie bars. The HSSs started to show local buckling at their base in a pattern similar to the buckling described previously for Specimen CFSSP-B1. Local buckling of the steel web plates and the HSS section occurred at different heights and were not linked. The welds between the tie bars and the CFSSP-B2 web were intact at that drift level.

At 3.33% drift, the specimen flexural strength was 117% of M_P. The amplitude of the local buckling of the steel web and the HSS increased and cracks started to develop at the tie bars fillet welds, as shown in Fig. 9(k). Fracture of the tie bars fillet welding developed on the full or half-diameter of the tie bars.

At a lateral drift value of 4%, the cracks started to propagate from the tie bar circumference to the web plate of the specimen, as shown in Fig. 9(l). At the end the cycles at that drift, the wall, although fractured along its base, still resisted 108% of M_P. The specimen was then pushed to a lateral drift of 4.67% to observe the reduction in flexural strength as a function of crack propagation.

After the end of the test, the specimen was cut; again, the concrete in the vicinity of the buckled steel plates was found to be crushed, but not elsewhere. The steel fibers added to the concrete mix to potentially enhance the ductility of the system were observed to have pulled out of the concrete at the crack location, suggesting that the steel fibers slipped from the concrete and possibly did not provide much benefits (the addition of steel fibers was done somewhat arbitrarily; pullout of the steel fibers from the concrete suggests an insufficient anchorage length). Whether or not the fibers allowed a better distribution of cracking along the wall height could not be verified, but that is a minor point given that, in this particular case, the use of fibers did not have a noticeable impact of the ultimate failure mode.

Local Buckling and Failure Modes

All specimens developed a similar ultimate behavior, with local buckling developing during ductile response while sustaining a lateral load with minimal strength degradation up to large drifts. Fracture in all specimens developed upon repeated cycles of local buckling of the steel web plate and of the HSS, and accelerated by fracture of the welding between the tie bars and skin plate. However, in all cases the vertical weld between the steel webs and the (half or full) HSS sections remained intact. In all cases, the cracks that developed in the metal after the development of local buckling only propagated upon development of larger drifts. This made it possible for the specimens to survive up to the large drifts recorded. Arguably, whether the crack propagation behavior would be different under dynamic loading is unknown at this time and could be the subject of future research. However, evidence collected during large-scale experiments of moment-resisting connections that fractured during the Northridge earthquake (Bruneau et al. 2011) suggested that dynamic response might not be significantly different from that observed during pseudostatic testing. Review of the videos recorded during the experiments showed that for Specimen CFSSP-B2, fracture started independently on the HSS at a different location, and that the wall would have failed at the same drifts even if fracture had not developed slightly earlier at the ties. This indicates that using a different welded or bolted detail for the tie bar to skin plate connection would not have significantly improved the behavior of the tested walls beyond what was obtained for Specimen CFSSP-B2 (provided that the tie bars in all cases are designed to have adequate strength and stiffness).

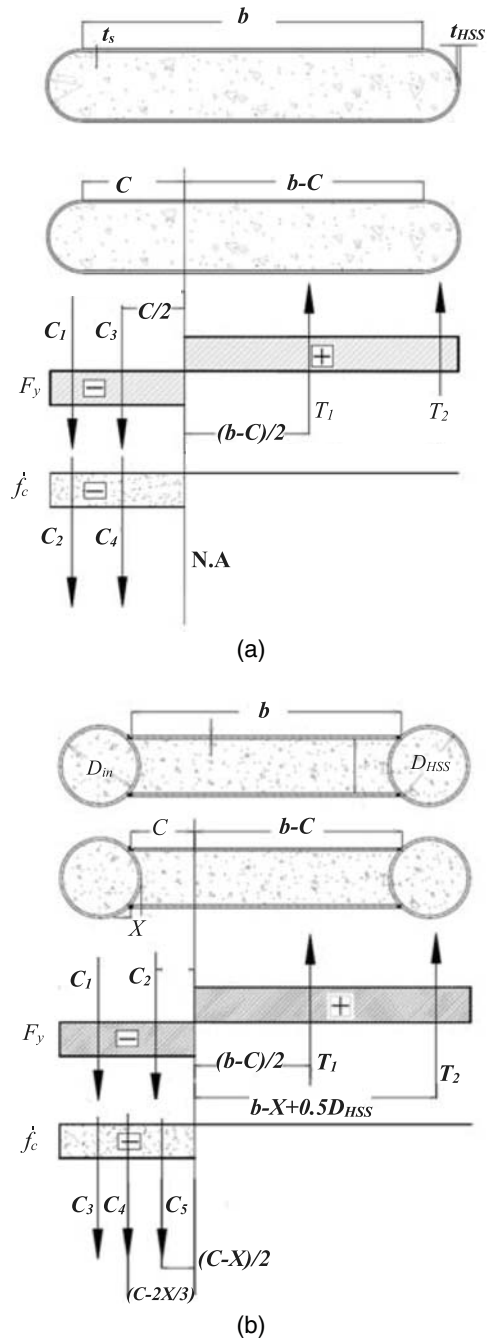

Fig. 10. Schematic diagram for the stress distribution used to calculate M_P: (a) CFSSP-NB cross section; (b) CFSSP-B cross section

Ductility Evaluation

Four of the tested specimens were able to sustain their strength up to drifts higher than 3%. Displacement ductility ratio, μ_D, was calculated based on the ratio between the maximum displacement, Δ_{max} (corresponding to 80% of the peak load), and the yield displacement, Δ_y (calculated from the idealized elastic-perfectly plastic envelope curve). Table 3 presents the ductility ratio values for the tested specimens. Displacement ductility exceeded 5.0, except for Specimen CFSSP-NB2, which reached a value closer to 4 (i.e., 3.67). Also, curvature ductility for the tested specimens was calculated from the experimentally recorded rotations, θ. Two curvature ductility values were calculated: one based on yield curvature defined from the idealized elastic-plastic envelope of the resulting moment curvature hysteretic curves, and another based on yield curvature defined by first yield at the extreme fiber of the HSS boundary element. Further details on curvature calculation are presented in Alzeni and Bruneau (2014).

Load-Carrying Capacity

The plastic moment capacity of the CFSSP walls was calculated using simple plastic theory principles, considering that the steel parts of the cross section have fully yielded on both the tension and compression sides of the plastic neutral axis, and that the concrete on the compression side has reached f'_c (neglecting any reduction factors), as shown in Fig. 10. Closed-form expressions derived to calculate the length of web subjected to compressions stresses, c, and the plastic moment, M_p, are presented as Eqs. (2) and (3) for CFSSP-NB walls, and Eqs. (4) and (5) CFSSP-B walls. Plastic moments calculated according to these equations are compared with experimental results in Table 4. It is observed that all of the tested specimens sustained a lateral load higher than that corresponding to development of the plastic moment at the base of the wall [calculated with Eqs. (2)–(5)]. Also in Table 4, the drift at which M_p and M_{max} is achieved is reported together with the ratio c/b, which represents the length of the web under compression, c, divided by the full length of the steel web, b

$$c = \frac{2bt_sF_{y,web} - 0.125(\pi d_{in}^2)f'_c}{4t_sF_{y,web} + t_cf'_c} \tag{2}$$

$$M_P = 0.5A_{HSS}F_{y,HSS}\left(\frac{2d_{HSS}}{\pi} + b\right) + (b^2 + 2c^2 - 2cb)t_sF_{y,web} + \left(\frac{2d_{in}^3 + 3\pi d_{in}^2 c}{24} + \frac{c^2t_c}{2}\right)f'_c \tag{3}$$

$$c = \frac{2bt_sF_{y,web} + (0.67Xt_c - 0.25\pi d_{in}^2)f'_c}{4t_sF_{y,web} + t_cf'_c} \tag{4}$$

Table 4. Load-Carrying Capacity of the CFSSP Walls

Specimens	Maximum strength M_{max} (kN-m)	Estimated M_p (kN-m)	M_{max}/M_p	Drift percent at M_{max} (%) M_p	Drift percent at M_{max} (%) M_{max}	c/b
CFSSP-NB1	4,1330.9	3,6200.2	1.13	1.20	1.80	0.25
CFSSP-NB2	4,1352.2	3,6200.2	1.13	1.20	1.80	0.25
CFSSP-B1	3,8042.1	3,0998.2	1.22	1.0	2.0	0.27
CFSSP-B2	3,8749.2	3,0998.2	1.25	1.0	2.67	0.27

$$M_p = A_{HSS}F_{y,HSS}(b - 2X + d_{HSS}) + (b^2 + 2c^2 - 2bc)t_sF_{y,web} + [0.25\pi d_{in}^2(0.5d_{HSS} + c - X) + 0.33Xt_c(c - 0.67X) + 0.5t_c(c - X)^2]f'_c \tag{5}$$

Summary and Conclusions

Four cantilever CFSSP walls, with and without boundary elements, were tested in order to evaluate their seismic performance. In walls without boundary elements, the cross section was closed at its ends by half-HSS sections; full HSS columns were used at the ends of the cross section for walls with boundary elements. The HSS sections met the AISC compactness requirements for moderate ductility, and spacing of ties was limited to 38 times the web plate thickness.

The tested walls were able to attain their plastic moment capacity, M_p, and all exhibited a ductile behavior through cyclic excursions with limited strength degradation up to 3% lateral drift. Local buckling of the steel web plates and/or the round HSS part of the cross section occurred only after the tested walls reached their M_p. The behavior of the specimens having a closer tie spacing of 25 times the web plate thickness was not significantly different. The value of M_p here was calculated by assuming that the steel has reached F_y in tension and compression on respective sides of the wall's neutral axis, and that the concrete over the entire compressed part of the wall has reached f'_c.

In all of the tested walls, fracture started in the steel web, after local buckling, typically initiating at the location of the connection between the tie bar and the web plate and propagating to the rest of the wall. In Specimen CFSSP-B2, which had tie bars fillet welded to the skin plates and exhibited an improved ductility, fracture simultaneously initiated in the HSS at a location independent from the steel web, which suggests that methods to connect the tie bars that would further delay fracture there would not, alone, enhance ductile behavior beyond that observed for Specimen CFSSP-B2.

Acknowledgments

This work was supported by AISC and the Egyptian Ministry of Higher Education. However, any opinions, findings, conclusions, and recommendations presented in this paper are those of the authors and do not necessarily reflect the views of the sponsors.

References

ABAQUS [Computer software]. Dassault Systemes, Providence, RI.
AISC. (2010). "Seismic provisions for structural steel buildings." *AISC 341*, Chicago.
AISC. (2016). "Seismic provisions for structural steel buildings." *AISC 341-16*, Chicago.
Alzeni, Y., and Bruneau, M. (2014). "Cyclic inelastic behavior of concrete filled sandwich panel walls subjected to in plane flexure." *Technical Rep. MCEER, 14-009*, MCEER Univ. at Buffalo, the State Univ. of New York, Buffalo, NY.
ASTM. (2010). "Standard specification for welded and seamless steel pipe piles." *ASTM A252*, West Conshohocken, PA.
ASTM. (2015). "Standard specification for high-strength low-alloy columbium-vanadium structural steel." *ASTM A572*, West Conshohocken, PA.
ASTM. (2017). "Standard test methods and definitions for mechanical testing of steel products." *ASTM A370*, West Conshohocken, PA.
ATC (Applied Technology Council). (1992). "The guidelines for cyclic seismic testing of components of steel structures." Redwood City, CA.

Bowerman, H., Gough, M., and King, C. (1999). *Bi-steel design and construction guide*, British Steel Ltd, Scunthorpe, U.K.

Bruneau, M., Uang, C. M., and Sabelli, R. (2011). *Ductile design of steel structures*, 2nd Ed., McGraw-Hill, New York, 921.

Cho, S. H., Tupper, B., Cook, W. D., and Mitchell, D. (2004). "Structural steel boundary elements for ductile concrete walls." *J. Struct. Eng.*, 10.1061/(ASCE)0733-9445(2004)130:5(762), 762–768.

Corus. (2003), *Bi-steel design and construction guide*, 2nd Ed., Corus UK Ltd., Scunthorpe, U.K.

Corus. (2007), "Fast steel cores." AISC, Modern Steel Construction Magazine, Chicago.

Dan, D., Fabian, A., and Stoian, V. (2011). "Theoretical and experimental study on composite steel-concrete shear walls with vertical steel encased profiles." *J. Constr. Steel Res.*, 67(5), 800–813.

El-Bahey, S., and Bruneau, M. (2011). "Bridge piers with structural fuses and bi-steel columns. I: Experimental testing." *J. Bridge Eng.*, 10.1061/(ASCE)BE.1943-5592.0000234, 25–35.

Eom, T.-S., Park, H.-G., Lee, C.-H., Kim, J.-H., and Chang, I.-H. (2009). "Behavior of double skin composite wall subjected to in-plane cyclic loading." *J. Struct. Eng.*, 10.1061/(ASCE)ST.1943-541X.0000057, 1239–1249.

Epackachi, S., Nguyen, N. H., Whittaker, A. S., and Varma, A. H. (2014). "In-plane seismic behavior of rectangular steel-plate composite wall piers." *J. Struct. Eng.*, 10.1061/(ASCE)ST.1943-541X.0001148, 04014176.

Ge, H., and Usami, T. (1996). "Cyclic tests of concrete-filled steel box columns." *J. Struct. Eng*, 10.1061/(ASCE)0733-9445(1996)122:10(1169), 1169–1177.

Hossain, K. A., and Wright, H. D. (1998). "Performance of profiled concrete shear panels." *J. Struct. Eng.*, 10.1061/(ASCE)0733-9445(1998)124:4(368), 368–381.

Kawashima, K., and Unjoh, S. (1997). "The damage of highway bridges in the 1995 Hyogo-Ken Nanbu earthquake and its impact on Japanese seismic design." *J. Earthquake Eng.*, 1(3), 505–541.

Kurt, E. G., Varma, A. H., Booth, P. N., and Whittaker, A., (2016). "In-plane behavior and design of rectangular SC wall piers without boundary elements." *J. Struct. Eng.*, 10.1061/(ASCE)ST.1943-541X.0001481, 04016026.

Liao, F.-Y., Han, L.-H., and Tao, Z. (2012). "Performance of reinforced concrete shear walls with steel reinforced concrete boundary columns." *Eng. Struct.*, 44, 186–209.

Lin, Y. C., and Tsai, K. C. (2004). "Seismic responses of steel shear wall constructed with restrainers." *Technical Rep. NCREE-04-015*, National Center for Research on Earthquake Engineering, Taipei, Taiwan (in Chinese).

Rahai, A., and Hatami, F. (2009). "Evaluation of composite shear wall behavior under cyclic loadings." *J. Constr. Steel Res.*, 65(7), 1528–1537.

Ramesh, S., Kreger, M. E., and Bowman, M. D. (2013). "Behavior and design of earthquake-resistant dual-plate composite shear wall systems." ⟨http://www.pankowfoundation.org/grants.cfm?prodonly=1⟩ (May 24, 2013).

Roeder, C. W., Macrae, G., Gunderson, C., and Lehman, D. (2003). "Seismic design criteria for CFT braced frame connections" *Proc., Int. Workshop on Steel and Concrete Composite Construction*, Taipei, Taiwan, 97–106.

Sener, K., and Varma, A. H. (2014). "Steel-plate composite SC walls: Experimental database and design for out-of-plane shear." *J. Constr. Steel Res.*, 100, 197–210.

Sener, K., Varma, A. H., and Ayhan, D. (2016). "Steel-plate composite SC walls: Experimental database and design for out-of-plane flexure." *J. Constr. Steel Res.*, 108, 46–59.

Seo, J., Varma, A. H., Sener, K., and Ayhan, D. (2016). "Steel-plate composite (SC) walls: In-plane shear behavior, database, and design." *J. Constr. Steel Res.*, 119, 202–215.

Usami, T., and Ge, H. (1994). "Ductility of concrete-filled steel box columns under cyclic loading." *J. Struct. Eng*, 10.1061/(ASCE)0733-9445(1994)120:7(2021), 2021–2040.

Varma, A. H., Malushte, S., Sener, K., and Lai, Z. (2014). "Steel-plate composite (SC) walls for safety related nuclear facilities: Design for in-plane force and out-of-plane moments." *Nucl. Eng. Des.*, 46(8), 240–249.

Wright, H. (1995). "Local stability of filled and encased steel sections." *J. Struct. Eng.*, 10.1061/(ASCE)0733-9445(1995)121:10(1382), 1382–1388.

Wright, H. (1998). "Axial and bending behavior of composite walls." *J. Struct. Eng.*, 10.1061/(ASCE)0733-9445(1998)124:7(758), 758–764.

Zhang, K., Varma, A. H., Malushte, S., and Gallocher, S. (2014). "Effects of shear connectors on the local buckling and composite action in steel concrete composite walls." *Nucl. Eng. Des.*, 46(8), 231–239.

Zhao, Q., and Astaneh-Asl, A. (2004). "Cyclic behavior of traditional and innovative composite shear walls." *J. Struct. Eng.*, 10.1061/(ASCE)0733-9445(2004)130:2(271), 271–284.